ADVANCED MATERIALS
www.advmat.de

Efficient White Electroluminescence from Cu-based Perovskite Achieved by High Hole Injection Core/Shell Structures

*Dongyu Li, Benzheng Lyu, Zhiwei Long, Xiangtian Xiao, Dongwei Zhang, Jiayun Sun, Qi Xiong, Zhengyan Jiang, Yufeng Wang, and Wallace C.H. Choy**

The copper-based (Cu-based) halide perovskite possesses eco-friendly features, bright self-trapped-exciton (broadband) emission, and a high color-rendering index (CRI) for achieving white emission. However, the limited hole injection (HI) of Cu-based perovskites has been bottle-necking the efficiency of white electroluminescence and thus their application in white perovskite light-emitting diodes (W-PeLEDs). In this study, we demonstrate a p-type cuprous sulfide (Cu_2S) lattice-connectedly capping over $Cs_3Cu_2I_5$ to form lattice-matched core/shell nanocrystals (NCs) by controlling the reactivity of sulfur (S) precursor in the synthesis. Interestingly, the resultant $Cs_3Cu_2I_5/Cu_2S$ NCs significantly enhance the hole mobility compared to $Cs_3Cu_2I_5$ NCs. Besides, the photoluminescence quantum yield of $Cs_3Cu_2I_5$ NCs increases from 26.8% to 70.6% after the Cu_2S lattice-connected capping. Consequently, by establishing the structure of $CsCu_2I_3/Cs_3Cu_2I_5/Cu_2S$ in W-PeLEDs, an external quantum efficiency of 3.45% and a CRI of 91 is realized, representing the highest reported electroluminescent performance in lead-free Cu-based W-PeLEDs. These findings contribute to establishing guidelines and effective strategies for designing broadband electroluminescent materials and device structures of PeLEDs.

1. Introduction

White light-emitting diodes (LEDs) have gained significant interest for their diverse applications in solid-state lighting and backlighting displays.[1–5] Typically, commercial white LEDs are realized by the photoluminescence (PL) of yellow phosphor or mixed red-green-blue phosphor coatings excited by blue LED chips.[6–8] However, these phosphors are often made from costly rare earth materials like Ce^{3+} or Eu^{3+}.[2,9] It is desirable to develop low-cost white electroluminescence (EL) materials with a large color rendering index (CRI), high photoluminescence quantum yield (PLQY), and stable spectra. Recently, multi-component composites based on different copper(I)-based halide perovskites have gained attention due to their bright self-trapped excitons (STEs) emission, high CRI, and eco-friendly features.[10–12] However, the blue-emitting component of $Cs_3Cu_2I_5$ with a large bandgap has poor hole injection and thus low EL efficiency of white light emission in combining with yellow STEs emission $CsCu_2I_3$ component.[13] Equally important, the hole mobility of the hole injection layer (HIL) is an order of magnitude lower than the electron mobility of typical electron injection material (EIL), resulting in severely unbalanced charge carrier injection in typically Cu-based white perovskite LEDs (W-PeLEDs).[14] The unbalanced charge carrier injection forms space charges in LEDs, leading to non-radiative recombination.[15] Consequently, it is crucial to improve the hole injection to the blue emissive component to achieve the desired W-PeLEDs.

D. Li, B. Lyu, Z. Long, J. Sun, Q. Xiong, Z. Jiang, W. C. Choy
Department of Electrical and Electronic Engineering
The University of Hong Kong
Pokfulam Road, Hong Kong 999077, P. R. China
E-mail: chchoy@eee.hku.hk

X. Xiao
School of Physics and Optoelectronic Engineering
Guangdong University of Technology
Guangzhou 510006, P. R. China

The ORCID identification number(s) for the author(s) of this article can be found under https://doi.org/10.1002/adma.202417678

DOI: 10.1002/adma.202417678

X. Xiao
Guangdong Provincial Key Laboratory of Sensing Physics and System Integration Applications
Guangdong University of Technology
Guangzhou 510006, P. R. China

D. Zhang, Y. Wang
Department of Chemistry
The University of Hong Kong
Pokfulam Road, Hong Kong 999077, P. R. China

J. Sun, Z. Jiang
Department of Electronic and Electrical Engineering
Southern University of Science and Technology
Shenzhen 518055, P. R. China

W. C. Choy
Materials Innovation Institute for Life Sciences and Energy (MILES)
HKU-SIRI
Shenzhen 518057, P.R. China

The core/shell heterostructure materials have been investigated to improve the optical properties, enhance the electron/hole injection, and reduce the surface-related trap states, which are beneficial from their applications in optoelectronic devices.[16–19] However, it is challenging to achieve high-quality core/shell structures in the perovskite system due to the vigorous nucleation and growth of perovskites hindering the formation of expected crystal structures and thus optoelectronic properties.[20,21] A slow formation of shell materials will prolong the reaction time, leading to the growth of too large perovskite crystals, while a fast formation results in a large number of shell materials, affecting the crystallization of perovskites.[22] Besides, when forming a shell material, there is an important issue of lattice mismatch. Particularly, when there is a larger lattice mismatch, there is a greater likelihood of increased defect density and lattice strain at the core/shell structures.[23] These factors can have a detrimental effect on the optoelectrical properties of the nanocrystals (NCs).[24,25] Therefore, careful optimization of the precursors to control the reactivity of the shell material and selection of the shell material to minimize lattice mismatch are crucial for the successful preparation of high-quality core/shell structures.

In this work, we successfully prepared high-quality core/shell structures by controlling the reactivity of sulfur (S) precursor in forming the shell layer. The resulting core/shell structure significantly enhances hole injection performance compared to pristine NCs. In addition, the core/shell structure can reduce the defect density and lattice strain of the core/shell structure, leading to a significant increase in PLQY from 26.8% to 70.6%. As a result, we achieve W-PeLEDs with a peak external quantum efficiency (EQE) of 3.45% and a high electroluminescence with brightness of 3356 cd m^{-2}, representing the best performance among reported lead-free W-PeLEDs. These findings contribute to preparing high-quality core/shell structures and improving the white EL properties for lighting/display applications.

2. Results and Discussion

2.1. Synthesis of $Cs_3Cu_2I_5/Cu_2S$ Core-Shell Structure

To achieve high-quality $Cs_3Cu_2I_5/Cu_2S$ core-shell structures, we propose a convenient one-pot thermal injection method by modulating the reactivity of the S precursor (**Figures** 1a and S1, Supporting Information). Conventional synthesis of core/shell structures in quantum dots adopts a two-step process, initiating the synthesis of the core layer before growing the shell layer, thus facilitating the formation of high-quality structures.[26] However, this method is not suitable for perovskites, as the two-step shell growth process requires high-temperature treatment. In the synthesis of the perovskite using the one-pot hot-injection method, it is necessary to terminate the growth of the core within a very short 30 s to prevent nanocrystal overripening from influencing the morphology and thus optical properties of the perovskite (Figure S2, Supporting Information). Therefore, it is essential to take into account the difference in growth rates between the core and shell layers to achieve the desired morphology and excellent optical properties in the synthesis of perovskite core-shell structures.

The S precursors (S-OA, S-OA/OAm, and S-OAm) were prepared by dissolving S powders in a mixture of ODE/OA, ODE//OA/OAm, and ODE/OAm, respectively (as detailed in the Experimental Section), where ODE denotes 1-octadecene, OA is oleic acid and OAm is oleylamine. The bonding between sulfur and coordinated functional groups primarily determines the reactivity of the S precursors.[27] The ^{1}H nuclear magnetic resonance (NMR) spectrum (Figure S3a, Supporting Information) reveals changes in resonance signals resulting from the interaction between sulfur and OAm since the lone pair of electrons of the nitrogen in OAm can coordinate with sulfur. There is no significant chemical shift in Figure S3b (Supporting Information), indicating that there is no interaction between sulfur and OA. According to the results of the ^{1}H NMR spectrum, the reactivity order of the three S precursors can be determined as S-OA > S-OA/OAm > S-OAm. Due to the ionic characteristics of perovskites, the core of the perovskite grows faster than the shell nucleation, making the core formation more pronounced, which is beneficial for establishing the perovskite core/shell structure.

The core-shell structure has been validated in the characterization of transmission electron microscopy (TEM) as shown in Figure 1b–d. When the reactivity of S precursor (S-OA) is high, the nucleation process of the shell and core may overlap in a period, leading to alternating growth, causing non-uniform morphology and size distribution of NCs (Figure 1b). When the reactivity of S precursor (S-OAm) is low, the nucleation and growth of Cu_2S may require more time. To ensure the quality of perovskite within the 30-s reaction time, termination of the reaction is necessary, while the nucleation and growth of Cu_2S may not have occurred yet, resulting in the formation of NCs similar to $Cs_3Cu_2I_5$ NCs, without the outer layer of Cu_2S coating, as shown in Figure 1d. These NCs also exhibit morphology similar to $Cs_3Cu_2I_5$ NCs, with a smaller particle size compared to $Cs_3Cu_2I_5/Cu_2S$ NCs. Meanwhile, with the appropriate reaction activation energy, we demonstrate the formation of the high-quality core-shell structures (Figure 1c). High-resolution TEM (HR-TEM) images show the same results, as shown in Figure 1e–g. $Cs_3Cu_2I_5$ NCs and Cu_2S exhibit distinct color appearances owing to their different electron beam penetration depth in Figure 1g. The lattice spacings of $Cs_3Cu_2I_5$ NCs and Cu_2S are calculated to be 3.38 A and 3.39 A, respectively, indicating a high 99.71% degree of lattice match. Equally important, HR-TEM images (Figure 1f) and the corresponding Fast Fourier transform (FFT, Figure S4, Supporting Information) show the lattice arrangement at the interface between Cu_2S (320) and $Cs_3Cu_2I_5$ (002), Cu_2S (100) and $Cs_3Cu_2I_5$ (222), indicating the shell lattice connected to the core. Theoretically, we also show the lattice connection of the lattice-matched Cu_2S shell to the $Cs_3Cu_2I_5$ core in the NCs as shown in Figure S5 (Supporting Information). The theoretical results show that the (002) planes of Cu_2S and the (222) planes of 0D $Cs_3Cu_2I_5$ NCs also exhibit a 99.71% degree of lattice match, which is consistent with the results of TEM. The core/shell structure of $Cs_3Cu_2I_5/Cu_2S$ shows well dispersion, good morphology, and bigger size (ave. 15.26 nm for the core/shell NCs as compared to ave. 13.04 nm in pristine $Cs_3Cu_2I_5$ NCs. Besides, the core/shell NCs show a narrower distribution (i.e., more uniform size) as compared to the pristine case shown in Figure S6 (Supporting Information).

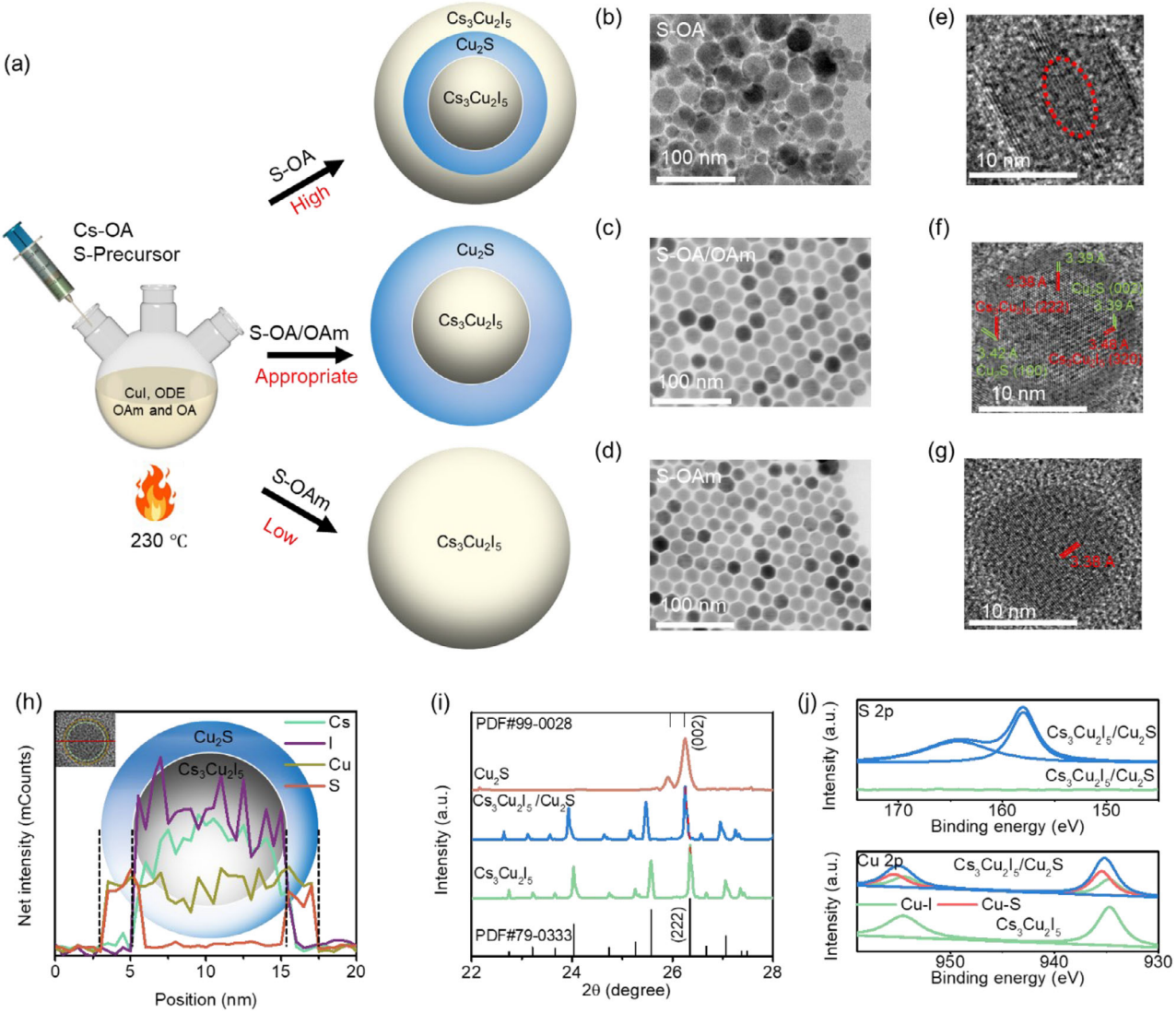

Figure 1. a) Synthesis reaction of $Cs_3Cu_2I_5/Cu_2S$ NCs using different S precursors. b–d) TEM images of Cu-based perovskite b) high-reactivity precursor, c) appropriate-reactivity precursor, and d) low-reactivity precursor. e–g) HR-TEM images of Cu-based perovskite e) high-reactivity precursor, f) appropriate-reactivity precursor, and g) low-reactivity precursor. h) Elemental line scan analysis curves for $Cs_3Cu_2I_5/Cu_2S$ NCs. i) XRD patterns of $Cs_3Cu_2I_5$ NCs, $Cs_3Cu_2I_5/Cu_2S$ NCs and Cu_2S. j) XPS spectra of $Cs_3Cu_2I_5$ NCs and $Cs_3Cu_2I_5/Cu_2S$ NCs.

The successful construction of the core/shell structure is also evidenced by EDS mapping and line scanning analysis, where Cu elements are distributed throughout the structure following the scribed line, and S elements are distributed around the Cs and I elements (Figures 1h and S7, Supporting Information). The X-ray diffraction (XRD) of the core/shell structure of $Cs_3Cu_2I_5/Cu_2S$ remains the same even after forming the Cu_2S shell, without any impurity phases. As demonstrated in Figure 1i, the XRD peaks exhibit a shift toward smaller angles due to the introduction of Cu_2S, which is consistent with the EDS results. To provide further evidence of the core/shell structure of Cu_2S coated $Cs_3Cu_2I_5$ NCs, X-ray photoelectron spectroscopy (XPS) was conducted to study the chemical environment of S and Cu elements (Figure 1j). The presence of two additional peaks at 164.3 and 158.1 eV in the S 2p spectrum of $Cs_3Cu_2I_5/Cu_2S$ indicates the successful binding of Cu_2S to the surface of $Cs_3Cu_2I_5$ through a strong chemical interaction between Cu in $Cs_3Cu_2I_5$ and S in Cu_2S. The peaks at 954.58 and 934.72 eV for $Cs_3Cu_2I_5$ NCs are assigned to the Cu 2p signal, which shifts toward higher binding energy upon incorporation of Cu_2S. The Cu 2p spectra for $Cs_3Cu_2I_5/Cu_2S$ NCs were fitted to Cu-S and Cu-I peaks, and the presence of Cu bonded to S (Cu-S) also confirmed the existence of Cu_2S on the $Cs_3Cu_2I_5$ NCs. In all, the above results proved that Cu_2S is indeed lattice-connectedly capped on the surface of $Cs_3Cu_2I_5$ NCs.

2.2. Electrical and Optical Properties of Cu_2S Coated $Cs_3Cu_2I_5$ NCs

To investigate the impact of Cu_2S coating on the electrical performance of $Cs_3Cu_2I_5$ NCs, the work function, valence band maximum (VBM), and band gap of $Cs_3Cu_2I_5$ and $Cs_3Cu_2I_5/Cu_2S$

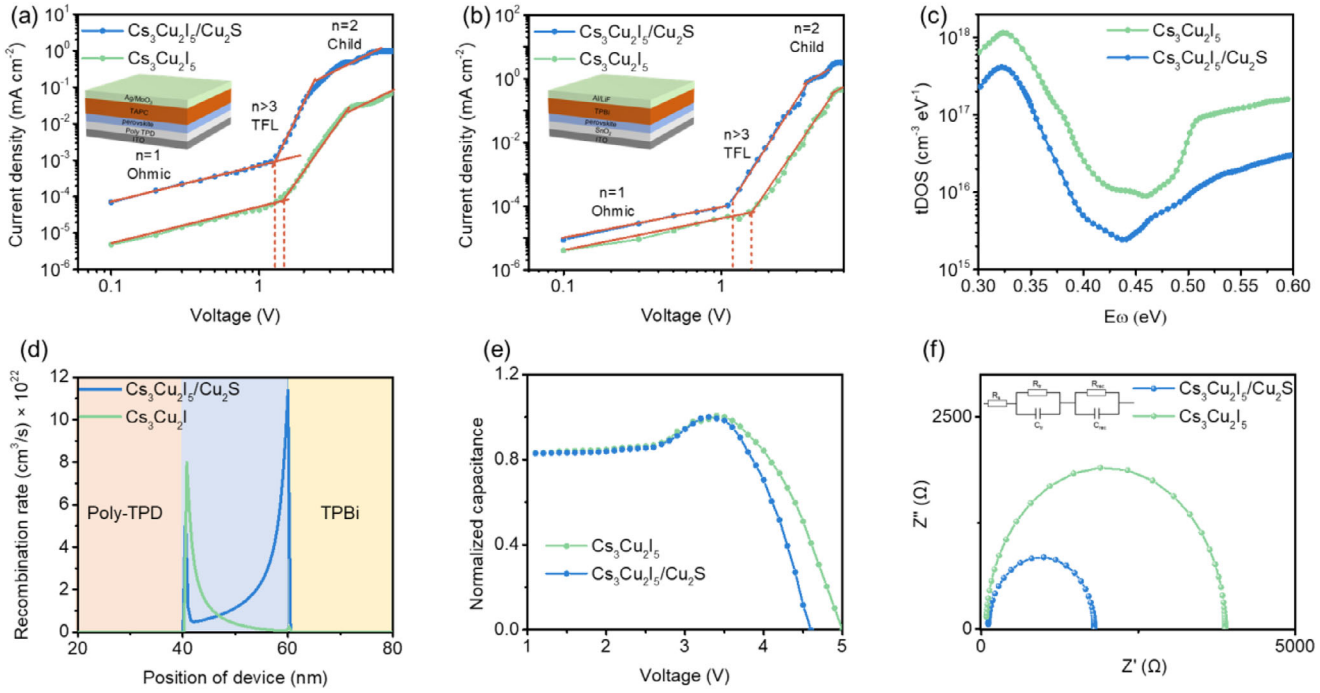

Figure 2. Current density-voltage characteristics of $Cs_3Cu_2I_5$ and $Cs_3Cu_2I_5/Cu_2S$ NC-based a) hole-only devices, and b) electron-only devices. c) tDOS of $Cs_3Cu_2I_5$ and $Cs_3Cu_2I_5/Cu_2S$ NCs. d) the simulated carrier recombination at a bias voltage 5 V for $Cs_3Cu_2I_5$ NCs and $Cs_3Cu_2I_5/Cu_2S$ NCs. e) the capacitance-voltage (*C–V*) plots $Cs_3Cu_2I_5$ NCs and $Cs_3Cu_2I_5/Cu_2S$ NCs. g) Nyquist plots of $Cs_3Cu_2I_5$ NCs and $Cs_3Cu_2I_5/Cu_2S$ NCs.

NCs, as well as Cu_2S, were determined using ultraviolet photoelectron spectroscopy (UPS, Figure S8, Supporting Information) and Tauc plots (Figure S9, Supporting Information). The VBM of $Cs_3Cu_2I_5$ was calculated as −6.51 eV and exhibited a gradual increase to −6.2 eV upon the incorporation of Cu_2S. The increased VBM could arise from a type-II band alignment between $Cs_3Cu_2I_5$ and Cu_2S. Additionally, Cu_2S exhibits a direct band gap of 2.66 eV and demonstrates p-type conductivity due to the gap of 0.4 eV between the VBM and Fermi energy. When Cu_2S is coated on $Cs_3Cu_2I_5$, a surface dipole exists at the interface between $Cs_3Cu_2I_5$ and Cu_2S, reducing the Fermi energy from −4.7 to −4.73 eV (Figure S10, Supporting Information). The decrease in Fermi energy level and the rise in the VBM lead to the gap decreasing from 1.81 to 1.47 eV, indicating a more pronounced p-type conductivity characteristic in $Cs_3Cu_2I_5/Cu_2S$. In addition, the energy levels alignment with the functional layer (hole transport layer and electron transport layer) is shown in Figure S11 (Supporting Information), indicating Cu_2S can reduce the energy barrier of hole injection from 1.11 to 0.8 eV. The p-type characteristic and reduction of the hole injection barrier facilitates the hole injection and is beneficial for balanced charge injections in electroluminescent devices, where the hole injection is typically more difficult than the electron injection.[28] The hole-only devices (ITO/Poly-TPD/perovskite/TAPC/MoO_3/Al) and electron-only devices (ITO/SnO_2/perovskite/TPBi/LiF/Al) of both materials under dark conditions were measured as shown in **Figure** 2a,b. Remarkably, the hole current density of $Cs_3Cu_2I_5/Cu_2S$-based devices is significantly enhanced by more than one order of magnitude due to the excellent HIL capability of Cu_2S. The trap densities of $Cs_3Cu_2I_5$ and $Cs_3Cu_2I_5/Cu_2S$ NCs can be calculated by the equation of $N_{trap} = (2\varepsilon_0\varepsilon V_{TFL})/(eL^2)$,[29] where ε_0 and ε represent the vacuum and relative permittivity, respectively. V_{TFL} is trap-filled limit voltage, e is the elementary charge, and L is the thickness of the perovskite film. To determine the trap state density, the value of ε is estimated by the equation of $\varepsilon = (CL)/(\varepsilon_0 S)$, where the geometrical capacitance of C can be determined from the *C–V* curves (Figure S12, Supporting Information).[29] The trap state density based on hole-only and electron-only devices for $Cs_3Cu_2I_5/Cu_2S$ NCs were determined to 5.48×10^{17} and 5.01×10^{17} cm^{-3}, respectively, both of which are lower than those of $Cs_3Cu_2I_5/Cu_2S$ NCs (6.30×10^{17} and 6.69×10^{17} cm^{-3}). Furthermore, after introducing Cu_2S, the mobility (μ) of $Cs_3Cu_2I_5/Cu_2S$ NCs increased to 1.76×10^4 from 4.6×10^3 cm^2 V^{-1} s^{-1} (hole) and to 2.58×10^4 from 6.48×10^3 cm^2 V^{-1} s^{-1} (electron), by substituting the current density (J) and voltage (V) in the Child region into the Mott-Gurney law equation: $\mu = 8L^3J/9\varepsilon_0\varepsilon V^2$.[29] These findings suggest that applying Cu_2S effectively enhanced the charge transport properties. The space charge limited current (SCLC) results further confirm the effective defect passivation of the perovskite film by Cu_2S. Additionally, the trap density of states (tDOS) of both perovskites was extracted from capacitance-frequency measurements on the devices (Figure S13, Supporting Information). As shown in Figure 2c, the $Cs_3Cu_2I_5/Cu_2S$ perovskite exhibits a much lower tDOS than the pristine perovskite over the entire energy range, consistent with the SCLC results, confirming the effective defect passivation by Cu_2S. To investigate the charge transfer and recombination capacity of $Cs_3Cu_2I_5$ and $Cs_3Cu_2I_5/Cu_2S$ W-PeLEDs, theoretical studies of W-PeLEDs were performed in Figures 2d and S14

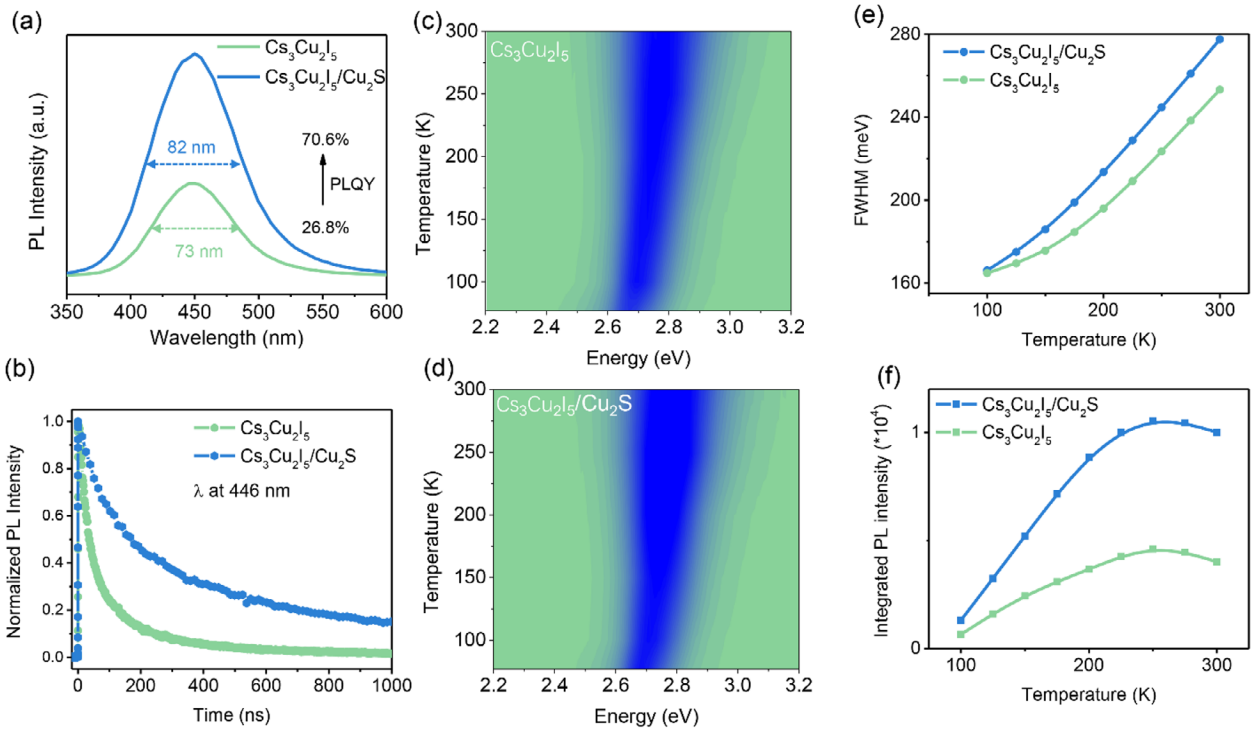

Figure 3. a) PL spectra and PLQY of $Cs_3Cu_2I_5$ NCs and $Cs_3Cu_2I_5/Cu_2S$ NCs, b) TRPL spectra and fitting for $Cs_3Cu_2I_5$ NCs and $Cs_3Cu_2I_5/Cu_2S$ NCs, c) PL spectra of $Cs_3Cu_2I_5$ NCs at different temperatures, d) PL spectra of $Cs_3Cu_2I_5/Cu_2S$ NCs at different temperatures, e) FWHM of $Cs_3Cu_2I_5$ NCs and $Cs_3Cu_2I_5/Cu_2S$ NCs at different temperatures, f) Integrated PL of $Cs_3Cu_2I_5$ NCs and $Cs_3Cu_2I_5/Cu_2S$ NCs at different temperatures.

(Supporting Information). The results show that the peak radiative recombination rate for $Cs_3Cu_2I_5/Cu_2S$-based W-PeLEDs increases to 1.2×10^{23} cm^3 s^{-1}, compared to 8×10^{22} cm^3 s^{-1} for pristine W-PeLEDs, which is consistent with the results of Figure 2a,b. To further verify the efficient charge transfer and high radiative recombination rate, capacitance-voltage (*C*–*V*) measurements were conducted (Figure 2e). The capacitance increases with increasing bias voltage, indicating more injected charges in the W-PeLEDs. At higher voltages, the capacitance sharply declines due to the radiative recombination of electrons and holes. The capacitance of $Cs_3Cu_2I_5/Cu_2S$-based W-PeLEDs decreases more rapidly than that of pristine W-PeLEDs when increasing the applied voltages, indicating more efficient charge transfer and radiative recombination in $Cs_3Cu_2I_5/Cu_2S$ NCs. Furthermore, electrochemical impedance spectroscopy (EIS) measurements were employed to elucidate the potential carrier transport behaviors in the devices. Figures 2f and S15 (Supporting Information) display the Nyquist plots of both devices against bias voltage under dark conditions, while the inset in Figure 2 illustrates the equivalent circuit.[30–32] The recombination resistance (R_{rec}) of the $Cs_3Cu_2I_5/Cu_2S$-based device is smaller than that of the control device (see Table S2, Supporting Information), indicating an increase in radiative recombination. Consequently, our findings demonstrate that efficient charge transfer in $Cs_3Cu_2I_5/Cu_2S$ NCs promotes greater radiative recombination of electrons and holes, resulting in brighter W-PeLEDs.

The broad spectral features observed in Cu-based perovskite NCs result from the STE emission induced by lattice distortion (**Figure 3a**). Incorporating Cu_2S can modify the lattice distortion, thereby strengthening the electron-phonon coupling and increasing the full width at half-maximum (FWHM) from 73 to 82 nm for white light applications. The absorption and PL excitation (PLE) spectra of $Cs_3Cu_2I_5$ NCs were altered upon the addition of Cu_2S due to Cu_2S-induced lattice distortion changes, thereby affecting the optical properties (Figure S16, Supporting Information). Compared to the reported Cu-based perovskite,[33–35] the initially synthesized perovskite before purification also displays a high PLQY of 90%, attributed to the abundance of ligands on its surface. These ligands effectively suppress the nonradiative recombination of the perovskite, resulting in a high PLQY. The poor conductivity of these ligands with long carbon chains significantly degrades the electrical properties of $Cs_3Cu_2I_5$ NCs, hindering their electroluminescence applications. Additionally, an excessive amount of surface ligands on perovskite will also lead to poor film formation and thus degrade device performance. By removing these ligands through purification, the enhancement of both electrical properties and film quality of $Cs_3Cu_2I_5$ NCs was achieved in this study. Then, we further developed the lattice-matched core/shell $Cs_3Cu_2I_5/Cu_2S$ NCs to increase the PLQY of $Cs_3Cu_2I_5/Cu_2S$ NCs from 26.8% to 70.6% and the hole mobility from 4.6×10^3 to 1.76×10^4 cm^2 V^{-1} s^{-1} promoting the performances of the W-PeLEDs. After being stored in 50% relative humidity (RH), 30 °C for 30 days, $Cs_3Cu_2I_5/Cu_2S$ NCs still retain ≈90% of their initial PLQY value (Figure S17, Supporting Information). Notably, even under heating at 100 °C or 100% RH, it can maintain 90% PLQY after 12 h. Notably, even under heating at 100 °C or underwater,

it can maintain 90% PLQY after 12 h. This finding highlights the capability of lattice-matched Cu_2S coating to enhance the stability of $Cs_3Cu_2I_5$ NCs. To investigate the mechanism of the PL enhancement in the core/shell NCs, we measure the time-resolved PL (TRPL) and study the exciton dynamics in $Cs_3Cu_2I_5$ NCs (as shown in Figure 3b). The increase in the average lifetime (τ_{avg}) from 175.9 to 401.5 ns indicated less trap-mediated nonradiative recombination in $Cs_3Cu_2I_5/Cu_2S$ NCs.[36,37] The $Cs_3Cu_2I_5$ NCs without Cu_2S coating exhibit a shorter lifetime due to a lower PLQY. The TRPL is studied using the equations:[38]

$$\tau = \frac{1}{k_r + k_{non}} \tag{1}$$

$$PLQY = \frac{k_r}{k_r + k_{non}} \tag{2}$$

where k_r and k_{non} are the radiative and non-radiative rates, respectively. The radiative and non-radiative rates for both samples were calculated and are summarized in Table S1 (Supporting Information), indicating an increase in radiative recombination rate from 1.5×10^{-3} to 1.8×10^{-3} ns^{-1}. The photoluminescence of Cu-based perovskite stems from STE induced by lattice distortion, and the modification with Cu_2S can influence lattice distortion, leading to enhanced radiative recombination in $Cs_3Cu_2I_5/Cu_2S$. The faster radiative recombination of STEs makes the lifetime of $Cs_3Cu_2I_5/Cu_2S$ NCs in the nanosecond range. Temperature-dependent PL was conducted on both $Cs_3Cu_2I_5/Cu_2S$ NCs and pristine $Cs_3Cu_2I_5$ NCs to investigate and quantify the optical properties. As shown in Figure 3c,d, the PL spectra of both samples broaden and exhibit a blue shift with increasing temperature. The correlated spectral responses of PL to temperature confirm that the PL originates from STE states. The temperature-dependent FWHM of the PL spectra (Figure 3e) as a function of temperature is studied using the phonon spectral width Equation:[39]

$$FWHM = 2.36\sqrt{S}E_{phonon}\sqrt{\coth\left(\frac{E_{phonon}}{2k_BT}\right)} \tag{3}$$

where S is the Huang-Rhys factor, T is the temperature, k_B is the Boltzmann constant, ω is the phonon frequency, and E_{phonon} is the phonon energy. The fittings of this equation to the experimental data are shown in Figure 3e, yielding S factors of 24 and 41.8, and E_{phonon} values of 20.6 and 30.8 meV for pristine $Cs_3Cu_2I_5$ NCs and $Cs_3Cu_2I_5/Cu_2S$ NCs, respectively. The large S factors of $Cs_3Cu_2I_5/Cu_2S$ NCs indicate the strong electron-phonon coupling during exciton self-trapping processes, leading to enhanced radiative recombination, which is consistent with previous studies.[40] Additionally, the integrated PL intensity initially increases with temperature and then decreases at higher temperatures, as shown in Figure 3f. This phenomenon, known as "negative thermal quenching," has been observed in semiconductors[41] and metal halides.[42] By further analyzing using the Shibata model correlating the two competing processes of thermal quenching and negative thermal quenching, the temperature-dependent PL intensity of both samples is modeled by the following equation:[43]

$$I\ (T) = I_0\ \frac{1 + Cexp\left(-\frac{E_c}{k_BT}\right)}{1 + Aexp\left(-\frac{E_a}{k_BT}\right) + Bexp\left(-\frac{E_b}{k_BT}\right)} \tag{4}$$

where I_0 is the integrated PL intensity at 0 K. The activation energy E_b is the exciton binding energy, while E_a is the self-trapped depth and the mechanism of self-trapped excitons (STEs) transitioning to free exciton states. E_c characterizes the negative thermal quenching effect on the PL intensity. From the studies, $Cs_3Cu_2I_5/Cu_2S$ NCs show Ea ≈3.8, Eb ≈189.6, and Ec ≈13.8 meV. For $Cs_3Cu_2I_5$ NCs, the refined constants are Ea ≈1.5, Eb ≈168.5, and Ec ≈12.6 meV. The greater self-trapped depth (E_a) and exciton binding energy of $Cs_3Cu_2I_5/Cu_2S$ NCs decrease the likelihood of exciton dissociation into free carriers, making them prone to radiative recombination from STE. Consequently, these results confirm that the emission of both samples originates from STE, and the coating of Cu_2S leads to enhanced luminescence performance.

2.3. Device Performances of W-PeLEDs

Inspired by excellent optoelectronic properties, we combined the $Cs_3Cu_2I_5/Cu_2S$ NCs with $CsCu_2I_3$ nanorods to achieve white EL in the W-PeLEDs with a configuration of ITO/ PEDOT: PSS/ Poly-TPD/ perovskite/ TPBi/ LiF/ Al as shown in Figure S18 (Supporting Information). All devices were fabricated in the same batch for fair comparison. Due to the slow charge transport in the $Cs_3Cu_2I_5$ NCs, most excitons recombine in the yellow-light $CsCu_2I_3$ nanorods, resulting in weak blue light and strong yellow light in the warm white light with CIE (0.38, 0.37), as shown in **Figure** 4a. Incorporating Cu_2S can enhance the hole injection in $Cs_3Cu_2I_5$ NCs, allowing more excitons to recombine in the blue-emission $Cs_3Cu_2I_5/Cu_2S$ NCs than of $Cs_3Cu_2I_5$ NCs. The increased emission of the blue component ($Cs_3Cu_2I_5/Cu_2S$ NCs) can greatly improve the brightness of white light emission and also result in a transition from warm white light (0.38, 0.37) to pure white light (0.31, 0.32), as shown in Figure 4b. Figure 4c shows the current density (J) -voltage (V) -luminance (L) of W-PeLEDs. While the W-PeLEDs with mixed $Cs_3Cu_2I_5$ NCs with $CsCu_2I_3$ nanorods as the active layer show maximum luminance of 110.6 cd m^{-2}, the $Cs_3Cu_2I_5/Cu_2S$ core-shell NC-based W-PeLEDs remarkably enhances the maximum luminance by ≈30-fold, reaching a value of 3356 cd m^{-2}. The $Cs_3Cu_2I_5/Cu_2S$ NC-based W-PeLEDs show much higher current densities than that of $Cs_3Cu_2I_5$ NCs, further confirming the better carrier injection (contributed by better hole mobility and significant suppression of traps) in the former case. The maximum EQE of $Cs_3Cu_2I_5/Cu_2S$ NCs device at 3.45% is ≈5 times better than the pristine one (0.72%) as in Figure 4d. The W-PeLED performance statistics show good reproducibility for the case of $Cs_3Cu_2I_5/Cu_2S$ NCs in Figure S19 (Supporting Information). Notably, to further confirm the similar J-V-L behavior due to the incorporation of Cu_2S shell, we also fabricated NC-only PeLEDs using $Cs_3Cu_2I_5$ NCs with and without Cu_2S shells. Our results in Figure S20 (Supporting Information) show similar trends

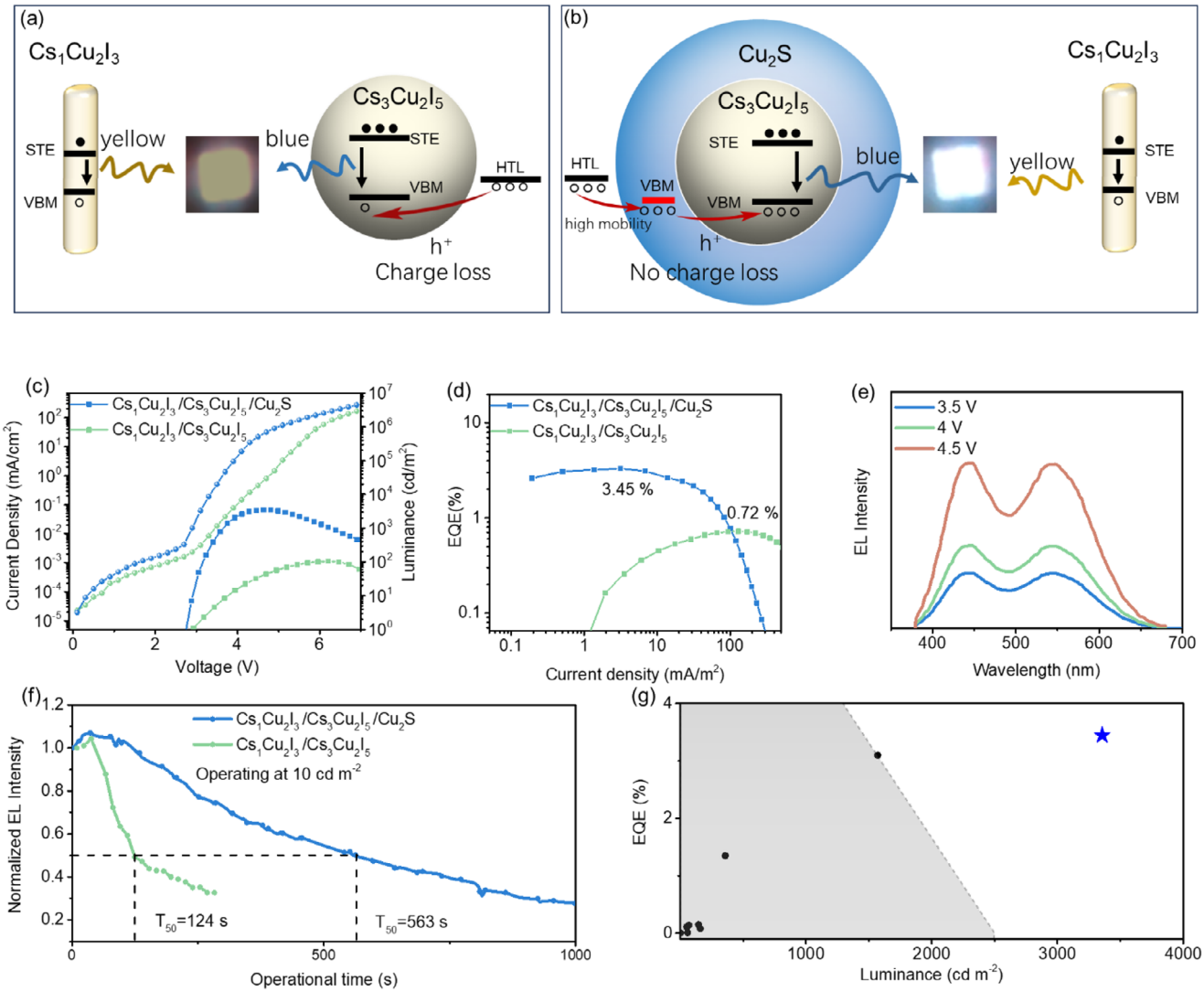

Figure 4. a,b) Illustration of the W-PeLED based on $Cs_3Cu_2I_5$ and $Cs_3Cu_2I_5/Cu_2S$ NCs, c) Current density-luminance-voltage characteristics of $Cs_3Cu_2I_5$ and $Cs_3Cu_2I_5/Cu_2S$ – W-PeLEDs, d) EQE curves as a function of the current density of $Cs_3Cu_2I_5$ and $Cs_3Cu_2I_5/Cu_2S$ – W-PeLEDs, e) EL spectra of $Cs_3Cu_2I_5/Cu_2S$ – W-PeLEDs, f) Stability of $Cs_3Cu_2I_5$ and $Cs_3Cu_2I_5/Cu_2S$ – W-PeLEDs at an initial luminance of 10 cd m^{-2}, g) Summary of the reported W-PeLEDs characteristics based on maximum EQE and estimated or measured luminance; the references in (g) are listed in Table S3 (Supporting Information).

to the W-PeLED that the blue PeLEDs of $Cs_3Cu_2I_5/Cu_2S$ NC PeLED show significantly enhanced as Cu_2S greatly improves the hole injection. Regarding the emission color (Figures 4e and S21, Supporting Information), the white EL of the W-PeLEDs with $Cs_3Cu_2I_5/Cu_2S$ NCs shows Commission Internationale de l'Eclairage (CIE) of (0.31, 0.32), and a high color rendering index (CRI) of 91 (Figure S22, Supporting Information). The CIE exhibits a slight shift from (0.31, 0.32) at 3.5 V to (0.32, 0.32) at 4.5 V and the CRI decreases from 91 to 90. The operational half-lifetime (T_{50}) value of the W-PeLEDs with Cu_2S coating is 563 s, which is four times longer than that of the control (Figure 4f). There is a gradual increment in the first few seconds. Such increasing performance can be attributed to the defect's self-healing behavior under electric fields.[44] Initially, the defects in the device will decrease because of the self-healing under electric fields, leading to a gradual increment in performance.[45,46] It is worth noting that the EQE and luminance of $Cs_3Cu_2I_5/Cu_2S$ NCs exceeded all reported W-PeLEDs based on lead-free perovskite (Figure 4g; Table S3, Supporting Information). After being stored at 50% RH, 30 °C for 30 days, W-PeLEDs based on $Cs_3Cu_2I_5/Cu_2S$ NCs still maintain ≈90% of their initial luminescence, as shown in Figure S23 (Supporting Information). Consequently, the employment of Cu_2S shell comprehensively and considerably enhances the EL properties, including both EQE and stability of Cu-based W-PeLEDs.

3. Conclusion

In conclusion, we have successfully demonstrated the formation of the NC structure of a lattice-matched Cu_2S shell

atomically connected to the $Cs_3Cu_2I_5$ core by controlling the reactivity of the S precursor. The $Cs_3Cu_2I_5/Cu_2S$ nanocrystals remarkably enhance hole mobility as compared to pristine nanocrystals, with an increase in PLQY from 26.8% to 70.6% after coating with the Cu_2S shell. Regarding the device performances, $Cs_3Cu_2I_5/Cu_2S/CsCu_2I_3$W-PeLEDs with a peak EQE of 3.45% and the operational half-lifetime (T_{50}) of 563 s at an initial luminance of 100 cd m^{-2} with an improvement over 4 times, representing the best performance in reported lead-free W-PeLEDs. Consequently, the work contributes to not only advancing the approach for forming lattice-match core/shell NCs but also paving the way to high-performance copper-based composite films for white LED applications.

Supporting Information

Supporting Information is available from the Wiley Online Library or from the author.

Acknowledgements

This work is supported by the University Grant Council of the University of Hong Kong Grants (Grant# Large Equipment Fund 2022-23, 202111159113, and 2302101786). General Research Fund (Grant# 17211220, 7200021, 17200823, and 17310624) and Collaborative Research Fund (Grant No. C7035-20G). from the Research Grants Council (RGC), as well as Innovation and Technology Fund from Innovation and Technology Commission (Grant No. GHP/245/22SZ) of Hong Kong Special Administrative Region, China. The authors would like to thank Shiyanjia Lab (www.shiyanjia.com) for supporting XPS analysis. [Correction added on April 3, 2025, after first online publication: Tetual Errors has been corrected.]

Conflict of Interest

The authors declare no conflict of interest.

Data Availability Statement

The data that support the findings of this study are available from the corresponding author upon reasonable request.

Keywords

core/shell structure, lead-free perovskite, self-trapped excitons, white light-emitting diodes

Received: November 14, 2024
Revised: March 24, 2025
Published online: April 1, 2025

[1] J. Luo, X. Wang, S. Li, J. Liu, Y. Guo, G. Niu, L. Yao, Y. Fu, L. Gao, Q. Dong, C. Zhao, M. Leng, F. Ma, W. Liang, L. Wang, S. Jin, J. Han, L. Zhang, J. Etheridge, J. Wang, Y. Yan, E. H. Sargent, J. Tang, *Nature* **2018**, *563*, 541.
[2] R. Sun, P. Lu, D. Zhou, W. Xu, N. Ding, H. Shao, Y. Zhang, D. Li, N. Wang, X. Zhuang, B. Dong, X. Bai, H. Song, *ACS Energy Lett.* **2020**, *5*, 2131.
[3] J. Mao, H. Lin, F. Ye, M. Qin, J. M. Burkhartsmeyer, H. Zhang, X. Lu, K. S. Wong, W. C. H. Choy, *ACS Nano* **2018**, *12*, 10486.
[4] E. P. Yao, Z. Yang, L. Meng, P. Sun, S. Dong, Y. Yang, Y. Yang, *Adv. Mater.* **2017**, *29*, 1606859.
[5] J. Chen, J. Wang, X. Xu, J. Li, J. Song, S. Lan, S. Liu, B. Cai, B. Han, J. T. Precht, D. Ginger, H. Zeng, *Nat. Photonics* **2020**, *15*, 238.
[6] S. Hou, M. K. Gangishetty, Q. Quan, D. N. Congreve, *Joule* **2018**, *2*, 2421.
[7] J. Chen, H. Xiang, J. Wang, R. Wang, Y. Li, Q. Shan, X. Xu, Y. Dong, C. Wei, H. Zeng, *ACS Nano* **2021**, *15*, 17150.
[8] Z. Chen, Z. Li, Z. Chen, R. Xia, G. Zou, L. Chu, S.-J. Su, J. Peng, H.-L. Yip, Y. Cao, *Joule* **2021**, *5*, 456.
[9] G. Pan, X. Bai, D. Yang, X. Chen, P. Jing, S. Qu, L. Zhang, D. Zhou, J. Zhu, W. Xu, B. Dong, H. Song, *Nano Lett.* **2017**, *17*, 8005.
[10] Z. Ma, Z. Shi, D. Yang, Y. Li, F. Zhang, L. Wang, X. Chen, D. Wu, Y. Tian, Y. Zhang, L. Zhang, X. Li, C. Shan, *Adv. Mater.* **2021**, *33*, 2001367.
[11] H. Chen, L. Zhu, C. Xue, P. Liu, X. Du, K. Wen, H. Zhang, L. Xu, C. Xiang, C. Lin, M. Qin, J. Zhang, T. Jiang, C. Yi, L. Cheng, C. Zhang, P. Yang, M. Niu, W. Xu, J. Lai, Y. Cao, J. Chang, H. Tian, Y. Jin, X. Lu, L. Jiang, N. Wang, W. Huang, J. Wang, *Nat. Commun.* **2021**, *12*, 1421.
[12] X. Meng, S. Ji, Q. Wang, X. Wang, T. Bai, R. Zhang, B. Yang, Y. Li, Z. Shao, J. Jiang, K. L. Han, F. Liu, *Adv. Sci.* **2022**, *9*, 2203596.
[13] R. Chen, Z. Ren, Y. Liang, G. Zhang, T. Dittrich, R. Liu, Y. Liu, Y. Zhao, S. Pang, H. An, C. Ni, P. Zhou, K. Han, F. Fan, C. Li, *Nature* **2022**, *610*, 296.
[14] K. Lin, J. Xing, L. N. Quan, F. P. G. de Arquer, X. Gong, J. Lu, L. Xie, W. Zhao, D. Zhang, C. Yan, W. Li, X. Liu, Y. Lu, J. Kirman, E. H. Sargent, Q. Xiong, Z. Wei, *Nature* **2018**, *562*, 245.
[15] Z. K. Tan, R. S. Moghaddam, M. L. Lai, P. Docampo, R. Higler, F. Deschler, M. Price, A. Sadhanala, L. M. Pazos, D. Credgington, F. Hanusch, T. Bein, H. J. Snaith, R. H. Friend, *Nat. Nanotechnol.* **2014**, *9*, 687.
[16] C. Ye, J. Jiang, S. Zou, W. Mi, Y. Xiao, *J. Am. Chem. Soc.* **2022**, *144*, 8162.
[17] B. G. Jeong, J. H. Chang, D. Hahm, S. Rhee, M. Park, S. Lee, Y. Kim, D. Shin, J. W. Park, C. Lee, D. C. Lee, K. Park, E. Hwang, W. K. Bae, *Nat. Mater.* **2021**, *21*, 246.
[18] Z. Li, R. Wang, J. Xue, X. Xing, C. Yu, T. Huang, J. Chu, K. L. Wang, C. Dong, Z. Wei, Y. Zhao, Z. K. Wang, Y. Yang, *J. Am. Chem. Soc.* **2019**, *141*, 17610.
[19] C. Zhang, S. Wang, X. Li, M. Yuan, L. Turyanska, X. Yang, *Adv. Funct. Mater.* **2020**, *30*, 1910582.
[20] D. FerrerA, X. G Torres-Castro, S. Sepúlveda-Guzmán, U. Ortiz-Méndez, M. José-Yacamán, *Nano Lett.* **2007**, *7*, 1707.
[21] P. Reiss, M. Protiere, L. Li, *Small* **2009**, *5*, 154.
[22] W. Lu, X. Guo, Y. Luo, Q. Li, R. Zhu, H. Pang, *Chem. Eng. J.* **2019**, *355*, 208.
[23] Q. Zhang, Y. H. Song, J. M. Hao, Y. F. Lan, L. Z. Feng, X. C. Ru, J. J. Wang, K. H. Song, J. N. Yang, T. Chen, H. B. Yao, *J. Am. Chem. Soc.* **2022**, *144*, 8162.
[24] R. G. Chaudhuri, S. Paria, *Chem. Rev.* **2011**, *112*, 2373.
[25] C. Zhang, J. Chen, L. Kong, L. Wang, S. Wang, W. Chen, R. Mao, L. Turyanska, G. Jia, X. Yang, *Adv. Funct. Mater.* **2021**, *31*, 2100438.
[26] T. Meng, Y. Zheng, D. Zhao, H. Hu, Y. Zhu, Z. Xu, S. Ju, J. Jing, X. Chen, H. Gao, K. Yang, T. Guo, F. Li, J. Fan, L. Qian, *Nat. Photonics* **2022**, *16*, 297.
[27] G. Yijun, R. A. Samuel, D. B. Joshua, V. Javier, *ACS Nano* **2013**, *7*, 3616.
[28] J. Zhang, T. Zhang, Z. Ma, F. Yuan, X. Zhou, H. Wang, Z. Liu, J. Qing, H. Chen, X. Li, S. Su, J. Xie, Z. Shi, L. Hou, C. Shan, *Adv. Mater.* **2022**,*35*, 2209002.
[29] Z. Li, Z. Chen, Y. Yang, Q. Xue, H. L. Yip, Y. Cao, *Nat. Commun.* **2019**, *10*, 1027.

[30] R. Li, S. Zhang, H. Zhang, Z. Wang, X. Feng, Y. Du, T. Zhou, X. Chen, P. Liu, L. Liu, J. Zhang, Q. Chen, L. Xi, K. Zhao, S. F. Liu, Q. Tian, *Angew. Chem., Int. Ed. Engl.* **2024**, *63*, 202410600.
[31] H. Zhou, W. Wang, Y. Duan, R. Sun, Y. Li, Z. Xie, D. Xu, M. Wu, Y. Wang, H. Li, Q. Fan, Y. Peng, Y. Yao, C. Liao, Q. Peng, S. Liu, Z. Liu, *Angew. Chem., Int. Ed. Engl.* **2024**, *63*, 202403068.
[32] Y. Li, Y. Duan, Z. Liu, L. Yang, H. Li, Q. Fan, H. Zhou, Y. Sun, M. Wu, X. Ren, N. Yuan, J. Ding, S. Yang, S. Liu, *Adv. Mater.* **2024**, *36*, 2310711.
[33] N. Li, Z. Xu, P. Wang, F. Wu, L. Liu, A. Najar, Y. Liu, Z. Yang, S. Liu, *ACS Appl. Nano Mater.* **2023**, *6*, 11472.
[34] X. Meng, J. Jiang, X. Yang, H. Zhao, Q. Meng, Y. Bai, Q. Wang, J. Song, C. Katan, J. Even, W. W. Yu, F. Liu, *Angew. Chem., Int. Ed.* **2024**, *136*, 202411047.
[35] W. Zhang, Z. Chu, Ji Jiang, S. Zhang, H. Hao, T. Wei, X. Zhang, a. J. You, *Adv. Opt. Mater.* **2024**, *12*, 2400092.
[36] H. Sun, X. Yang, P. Li, Y. Bai, Q. Meng, H. Zhao, Q. Wang, Z. Wen, L. Huang, D. Huang, W. W. Yu, H. Chen, F. Liu, *Nano Lett.* **2024**, *24*, 10355.
[37] H. Zhao, Q. Wang, Z. Wen, H. Sun, S. Ji, X. Meng, R. Zhang, J. Jiang, Z. Tang, F. Liu, *Angew. Chem., Int. Ed.* **2023**, *62*, 202316336.
[38] D. Li, D. Zhou, W. Xu, X. Chen, G. Pan, X. Zhou, N. Ding, H. Song, *Adv. Funct. Mater.* **2018**, *28*, 1804429.
[39] Z. Xing, Z. Zhou, G. Zhong, C. C. S. Chan, Y. Li, X. Zou, J. E. Halpert, H. Su, K. S. Wong, *Adv. Funct. Mater.* **2022**, *32*, 2207638.
[40] L. Zhou, J. F. Liao, D. B. Kuang, *Adv. Opt. Mater.* **2021**, *9*, 2100544.
[41] Y. Wu, J. Li, H. Ding, Z. Gao, Y. Wu, N. Pan, X. Wang, *Phys. Chem. Chem. Phys.* **2015**, *17*, 5360.
[42] Y. Ling, L. Tan, X. Wang, Y. Zhou, Y. Xin, B. Ma, K. Hanson, H. Gao, *J. Phys. Chem. Lett.* **2017**, *8*, 3266.
[43] H. Zhang, L. Yang, H. Chen, W. Ma, R. Wang, G. Cao, *Mater. Chem. Front.* **2022**, *6*, 1647.
[44] D. R. Ceratti, Y. Rakita, L. Cremonesi, R. Tenne, V. Kalchenko, M. Elbaum, D. Oron, M. A. C. Potenza, G. Hodes, D. Cahen, *Adv. Mater.* **2018**, *30*, 1706273.
[45] W. Xu, Q. Hu, S. Bai, C. Bao, Y. Miao, Z. Yuan, T. Borzda, A. J. Barker, E. Tyukalova, Z. Hu, M. Kawecki, H. Wang, Z. Yan, X. Liu, X. Shi, K. Uvdal, M. Fahlman, W. Zhang, M. Duchamp, J.-M. Liu, A. Petrozza, J. Wang, L.-M. Liu, W. Huang, F. Gao, *Nat. Photonics* **2019**, *13*, 418.
[46] J. W. Lee, S. Tan, T. H. Han, R. Wang, L. Zhang, C. Park, M. Yoon, C. Choi, M. Xu, M. E. Liao, S. J. Lee, S. Nuryyeva, C. Zhu, K. Huynh, M. S. Goorsky, Y. Huang, X. Pan, Y. Yang, *Nat. Commun.* **2020**, *11*, 5514.